Inferring an Evolutionary Tree of Uveal Melanoma From Genomic Copy Number Aberrations

Nakul Singh,[1] Arun D. Singh,[2] and Winston Hide[3,4]

[1]School of Medicine, Case Western Reserve University, Cleveland, Ohio, United States
[2]Cole Eye Institute, Cleveland Clinic, Cleveland, Ohio, United States
[3]Biostatistics Department, Harvard School of Public Health, Boston, Massachusetts, United States
[4]Sheffield Institute for Translational Neuroscience, University of Sheffield, Sheffield, United Kingdom

Correspondence: Nakul Singh, Case Western Reserve University School of Medicine, 2109 Adelbert Rd, Cleveland, OH 44106, USA; nakul.singh@case.edu.

Submitted: March 7, 2015
Accepted: September 7, 2015

Citation: Singh N, Singh AD, Hide W. Inferring an evolutionary tree of uveal melanoma from genomic copy number aberrations. *Invest Ophthalmol Vis Sci*. 2015;56:6801–6809. DOI:10.1167/iovs.15-16822

Purpose. The purpose of this study is to study the genomic evolution of primary uveal melanoma.

Methods. Primary uveal melanoma genomic DNA was assayed on the Illumina Human660W-Quad v1.0 DNA Analysis BeadChip. Raw signal intensity data were quantile normalized to estimate copy number aberration with the Genome Alteration Print algorithm. Distance between samples was calculated as the Manhattan distance between the copy number profiles of the tumors. From the distance matrix, a phylogenetic network (evolutionary relationship inference) was estimated using SplitsTree4.

Results. Of the 57 tumors, one (1.8%) was discarded because of a failed assay, and seven (12.3%) were revealed to be mixtures of several cell populations that could not be resolved. Three clades of tumor were identified (A [59.2%], B [32.7%], and C [6.1%]), each following a distinct evolutionary path and each associated with metastatic status ($P = 0.01$). One tumor (2.0%) did not fit into any clade. From a normal diploid melanocyte, a few tumors (clade C) lose a large portion of chromosome 6q, but do not develop any mutations on 8q. In an alternate path, the vast majority of tumors (clade A and clade B [91.9%]) gain a copy of the telomeric half of 8q. A majority of these tumors (clade A) subsequently lose a copy of chromosome 3, as well as gain the centromeric half of 8q. The other tumors (clade B) gain copies of 6p, as well as regions on 11p and 22q.

Conclusions. Our data suggest that there is little overlap in the subtypes of uveal melanoma after divergence (identified as clades A and B) and that these distinct subtypes are not likely to crossover or transform from one major clade to another.

Keywords: molecular genetics; bioinformatics; uveal melanoma

Uveal melanoma is the most frequent primary intraocular malignant tumor in adults, wherein approximately half of all cases metastasize.[1] High-throughput studies of the disease have identified genetic mutations, patterns of chromosomal aberrations, and patterns of gene expression that are associated with metastatic risk.[2] Taken together, a preliminary sketch of the biology of uveal melanoma has been developed.[2] It is hypothesized that a normal uveal melanocyte first undergoes mutations in either the *GNAQ or GNA11* gene along its path to transformation to a uveal nevus,[3,4] followed by mutation in the *BAP1, EIF1AX,* or*SF3B1* gene.[5–7] Mutations in the *BAP1* gene are associated with monosomy 3 and a phenotype similar to an early-stage, undifferentiated stem cell–associated with a high risk of metastasis.[8] On the other hand, mutations in the *EIF1AX* and *SF3B1* genes are associated with a phenotype, which behaves similarly to a differentiated melanocyte, associated with a low risk of metastasis.[2]

This hypothetical sequence of events is difficult to formally test in humans, given the clinical infeasibility of sampling tumors repeatedly at various stages of development. To this end, we applied modeling strategies from the field of evolutionary biology, specifically phylogenetics, to trace the evolution of uveal melanoma. The goal of phylogenetics is to identify molecular events that define species and to estimate the order and timing of such genetic events. For example, phylogenetic analysis has been successfully applied to bacterial genomes to trace the evolution of genes responsible for antibiotic resistance. By comparing pathogenic and commensal bacteria genomes, it can be inferred that antibiotic resistance likely occurred before the antibiotic era and that the use of antibiotics has resulted in the selection of resistant species rather than induction of mutations that cause resistance.[9]

Similarly, by analyzing the patterns of copy number aberrations within tumor genomes, we can infer the sequence of copy number aberrations (mutations). Additionally, we may be able to identify patterns of copy number aberrations that define tumor subgroups of clinical significance, such as response to treatment, likelihood of metastasis, and mortality. Thus, the goal of this study was to develop an evolutionary tree of uveal melanoma. Methods that were designed to study the differentiation of species were adapted to infer the evolutionary relationship between several primary tumors using a cross-sectional genomics data set. The resulting tree revealed natural groupings of tumors, or "clades," as they are referred to in evolutionary biology. Clades experience similar genomic events as they evolve.

Materials and Methods

Samples

Primary tumor tissue was isolated from the enucleated eyes of 57 patients. Immediately following enucleation, transillumination was used to mark the tumor margins. Dissection was carried out through a scleral flap overlying the tumor base. Fresh tumor tissue was immediately frozen and stored at –80°C. Single nucleotide polymorphism (SNP) microarray analysis was performed on fresh frozen tumor tissue that was permeabilized in RNA protective reagent RNAlater-ICE (Ambion, Austin, TX, USA) per the manufacturer. Permeabilized tissue was minced, equilibrated in cold PBS, and then digested with proteinase-K prior to DNA extraction using the DNeasy kit (Qiagen, Germantown, MD, USA). Approximately 200 ng DNA per sample was assayed on the Illumina Human660W-Quad v1.0 BeadChip (Illumina, San Diego, CA, USA). Probe preparation and hybridization were performed by the Cleveland Clinic Genomics Core.[10] Raw assay signal data and clinical annotations were uploaded to the Gene Expression Omnibus (GEO) in February 2013, a publically available, online repository of data from array and sequence assays (GEO accession no. GSE44297). Data were downloaded in March 2013. Raw signal data were visualized to assess technical assay failure by the authors (NS and WH). Samples were excluded from analysis if data were washed out. The end point for follow-up was either last date of contact or date of death. The association between patient characteristics and metastatic status was tested by Fisher's exact test.

Copy Number Estimation

For each SNP assayed by the microarray, there are two alleles for each locus, with several probes that are designed to hybridize with each allele. When a probe hybridizes with the targeted allele from the sampled genome, the probe fluoresces. A laser scanner detects probe fluorescence intensity.[11]

The final raw microarray data consist of two fluorescence intensity measurements for each SNP such that each intensity measurement corresponds to the presence of a particular allele. However, on Illumina assays, there is a known bias in the signal measurement due to differential fluorescence between the two dyes used.[12] The threshold quantile normalization (tQN) algorithm was used to correct this bias by shifting the distribution of signal of one dye to closely match the distribution of signal of the other dye. This process is called quantile normalization, and it also ensures that extremely low or high values are not excluded.[12]

The normalized intensity data were then used to estimate copy number at a particular locus by determining the absolute intensity of both probes and the ratio of the intensity between the two probes.[13] For example, a genomic region that is associated with a 1:1 ratio of one allele to another, together with a total fluorescence that is around normal, would be inferred as a normal copy number region. A region with fluorescence intensity of 2:1 of one allele to another, along with a fluorescence intensity of 1.5 times the normal, suggests a copy number of 3 at that region. To ease in the computational task associated with estimating copy number status for more than 660,000 genomic locations, the Genome Alteration Print (GAP) algorithm first estimates regions of the genome that are likely to have similar copy number status before it estimates copy number status.[13] In this way, the copy number status (normal or aberrant [deleted or duplicated]) of every segment of the genome was inferred.

If there was evidence of multiple cell populations on the assay, as suggested by lack of consistent probe signal across adjoining SNPs,[13] samples were excluded. Excluded samples were tested for association with demographic and clinical features by Fisher's exact test. Visual inspection of the estimates revealed the algorithm could not reliably distinguish between single and double amplification events, corresponding to a copy number of 3 and 4, respectively, likely due to the saturation effects of the microarray assay.[14] All copy number estimates greater than, less than, and equal to 2 were coded as duplication, deletion, and copy neutral, respectively.

Distance Matrix Calculation

The genome was divided into segments, where each segment represented the longest contiguous length of genome that acted as a unit across all samples (Fig. 1). In this way, each segment represented a potential site for a copy number event. Such feature reduction techniques have been shown to improve statistical power by identifying important regions and thereby reducing the number of statistical tests required.[15] Differences in copy number values for each segment were tabulated. The sum of all differences is the Manhattan distance between two samples. The Manhattan distance therefore is a numeric representation of copy number differences between two samples. The Manhattan distance was calculated for every pair of tumor samples and for a "normal" diploid sample (Fig. 1). The normal diploid sample, in this case, was a synthetic entity wherein the entire genome was posited to have zero deletions or duplications, that is, having a copy number of 2 at all genomic segments. The normal diploid was set as the root of the network, the ancestor from which all other samples were derived.

Evolutionary Relationship Inference

From the Manhattan distances, a phylogenetic network (evolutionary relationship inference), specifically a neighborhood-net, was estimated using SplitsTree4 (Huson and Bryant, Tübingen, Germany).[16] A neighborhood-net is the summary of many different possible evolutionary trees, each of which is supported by the data. The network was visually inspected to determine the number of tumor clades. Clade membership was tested for association with demographic and clinical features. Fisher's exact test was used for categorical features, and the Kruskal-Wallis test was used to test difference in age distribution. The Kruskal-Wallis test was used, because it can be applied to more than two groups, and it is robust to nonnormal distributions and unequal sample sizes.

Identification of Defining Copy Number Aberrations

To identify copy number aberrations defining the clade, the copy number profiles of tumors within each hypothesized uveal melanoma clade were summed to generate a profile of the clade. Copy number aberrations that were present in more than 80% of the tumors within a clade were considered defining. Additionally, each segment was tested for an association with tumor clade by means of a Fisher's exact test using a Benjamini-Hochberg corrected P value of 0.05.[17] Additionally, the relative frequency of copy number aberrations of the segments that contained the genes *GNAQ, GNA11, BAP1,* and *SF3B1* was examined by clade. Gene locations were identified from University of California Santa Cruz Genome Browser.[18] The *EIF1AX* gene, located on chromosome Xp22, could not be examined as sex chromosomes were excluded in the analysis.

Investigative Ophthalmology & Visual Science

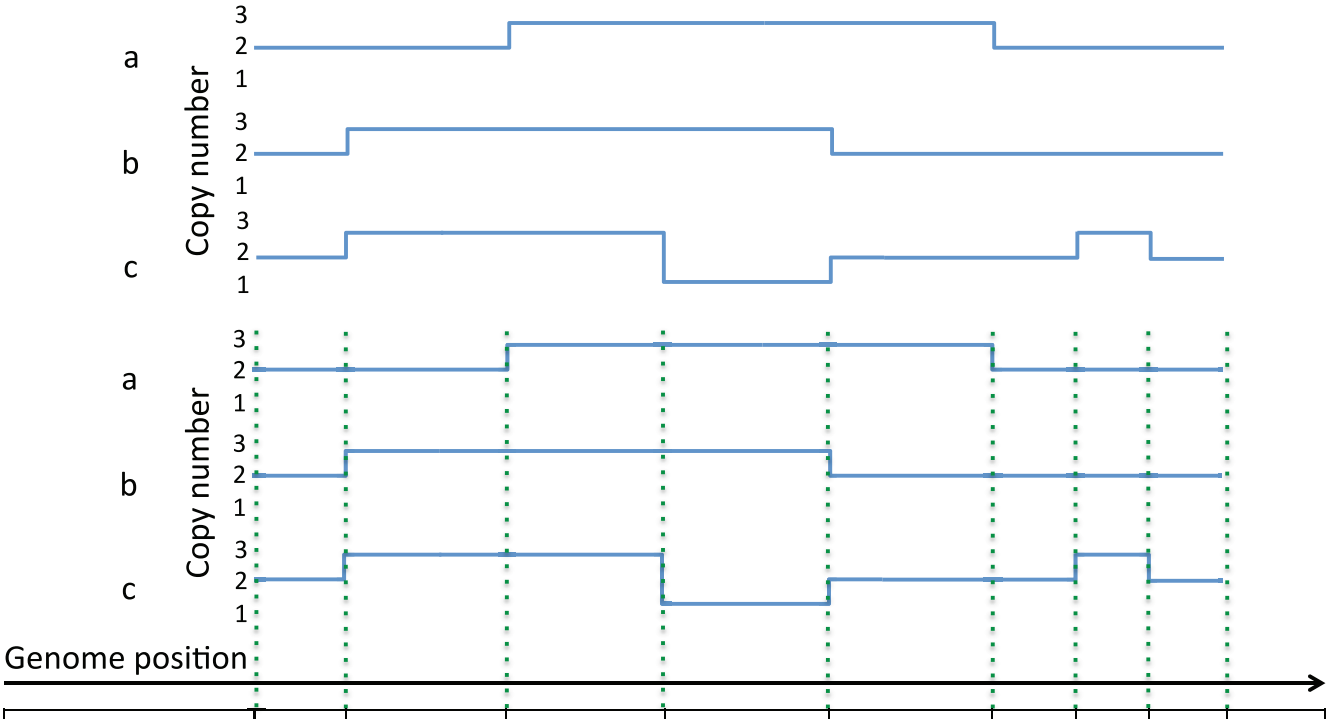

									Total
a	2	2	3	3	3	2	2	2	
b	2	3	3	3	2	2	2	2	
|Difference|	0	1	0	0	1	0	0	0	2

FIGURE 1. Distance matrix calculation. (*Top*) The copy number estimates of the entire genome from the GAP algorithm of three tumor samples (a, b, c). Copy number greater than, less than, and equal to 2 indicate duplication, deletion, and copy neutral status, respectively, in each tumor sample. (*Middle*) The genome was divided into segments, where each segment represented the longest contiguous length of genome that was aberrant as a unit across all tumor samples. (*Bottom*) Calculation of Manhattan distance between two samples (a and b). Difference in copy number value for each segment is tabulated. The sum of all differences is the Manhattan distance between two samples. Manhattan distance is a numeric representation of copy number differences between two samples. Manhattan distance is calculated for every pair of tumor samples.

Ancestral Reconstruction

The lists of defining mutated segments for each clade, as identified from the summed profile and Fisher's exact test analyses, were compared for overlaps and differences. Based on the assumption that copy number aberrations present in more than one clade occurred earlier than copy number aberrations present in a single clade, we developed a hypothetical evolutionary path of uveal melanoma defined by genomic events.

RESULTS

Sample Characteristics

Tumors were collected from 57 enucleated eyes. Demographic and clinical information is presented in Table 1. Of all patients, 25 (43.9%) were female, with an average age of 63.4 years (SD = 15.4). Twenty-seven (47.4%) tumors had metastasized, and 30 (52.6%) had not. Twenty-eight (49.1%) tumors had ciliary body involvement (iridociliary or ciliochoroidal tumors), and 29 (50.9%) were limited to the choroid. Of the 57 tumors, one (1.8%) was discarded because of a failed assay, and seven (12.3%) were determined to be mixtures of several cell populations that could not be resolved by the GAP algorithm. The remaining 49 (84.5%) tumors were included in the analysis. There were no differences in age, sex, metastatic status, or tumor location between samples included or excluded from the analysis. The median follow-up time for the entire cohort was 42.1 months (IQR = 36.0).

Additionally, there was no association between metastatic status, tumor location, or sex of the patients.

Copy Number Estimation

From more than 660,000 probes, GAP identified 2654 genomic segments whose copy number status captured all of the copy number information for all samples. The shortest segment contained four probes, and the longest segment contained 14,590 probes, with a mean segment length of 294.8 probes and median segment length of 32 probes. Chromosome 6 required 175 genomic segments to summarize its copy number information across all the samples, while chromosome 21 required only 25 segments; these chromosomes required the most and least segments, respectively.

The mean number of segments either amplified or deleted in the samples was 452 (21.0%), with a minimum of 76 (3.5%) and maximum of 1075 (49.1%). The mean number of segments amplified was 218 (10.1%), with a minimum of 29 (1.3%) and maximum of 1031 (47.9%). The mean number of segments

Investigative Ophthalmology & Visual Science

Table 1. Demographic and Clinical Information About Samples Studied

Parameter	Included	Discarded	*P* Value	Total	%
Age, mean (SD)	62.8 (2.2)	67.5 (5.0)	0.43	63.4 (15.3)	
Caucasian	49	8		57	100
Sex					
Male	28	4		32	56.1
Female	21	4	0.77	25	43.9
Location					
Ciliary body ± iris or choroid	25	3		28	49.1
Choroid only	24	5	0.70	29	50.9
AJCC classification					
1a	2	0		2	
2a	7	0		7	
2b	3	0		3	
3a	11	3		14	
3b	10	1		11	
4a	4	2		6	
4b	12	2	0.70	14	
Metastasis					
Present	23	4		27	47.4
Absent	26	4	1.00	30	52.6
Median follow-up time, months	49.1	26.5	0.04	42.0	

deleted was 234 (10.8%), with a minimum of 13 (0.6%) and maximum of 435 (22.3%).

Figure 2 shows the relative frequency of copy number aberrations for all samples included in the analysis. Table 2 presents the 10 most amplified and deleted regions of the 49 tumor samples. The most deleted segment occurred on chromosome 20. This segment was absent in 41 (83.7%) of the samples. The most amplified segment occurred on chromosome 8. This segment was amplified in 42 (85.7%) of the samples. The 10 most deleted segments were located on chromosome 20 and chromosome 3. The 10 most amplified segments were located on chromosome 8. There were 45 segments that were not mutated in any sample, and they all occurred on chromosomes 10, 17, and 19 (Supplementary Table S1).

Evolutionary Relationship Inference

There seemed to be two larger clades that comprised 29 (59.2%) and 16 (32.7%) samples, respectively (91.9%). An additional small clade was comprised of three (6.1%) samples. One sample (2.0%) was not in any obvious grouping. In the rest of this paper, the largest clade will be referred to as clade A, the second largest as clade B, and the smallest as clade C. The estimated phylogenetic network is shown in Figure 3.

Table 3 presents demographic and clinical features of the three clades. The clades were associated with metastatic status ($P = 0.01$ by Fisher's exact test). Clade A was characterized by an enrichment of metastatic samples (69.0%, 20 of 29). Clade B was composed of predominantly nonmetastatic tumors (87.5% nonmetastatic, 14 of 16), and clade C was a mixture of metastatic and nonmetastatic tumors (33.3% metastatic, 1 of 3). There was a borderline association between clade and tumor location ($P = 0.05$, Fisher's exact test). There was no association between clade and age of patient at diagnosis ($P = 0.14$, Kruskal-Wallis). Median follow-up time for patients in clades A, B, and C was 38.0, 61.0, and 53.0 months, respectively ($P = 0.05$, Kruskal-Wallis).

Identification of Defining Copy Number Aberrations

Copy number aberrations that occurred in more than 80% of tumors of a given clade are shown in Table 4. Regions near the

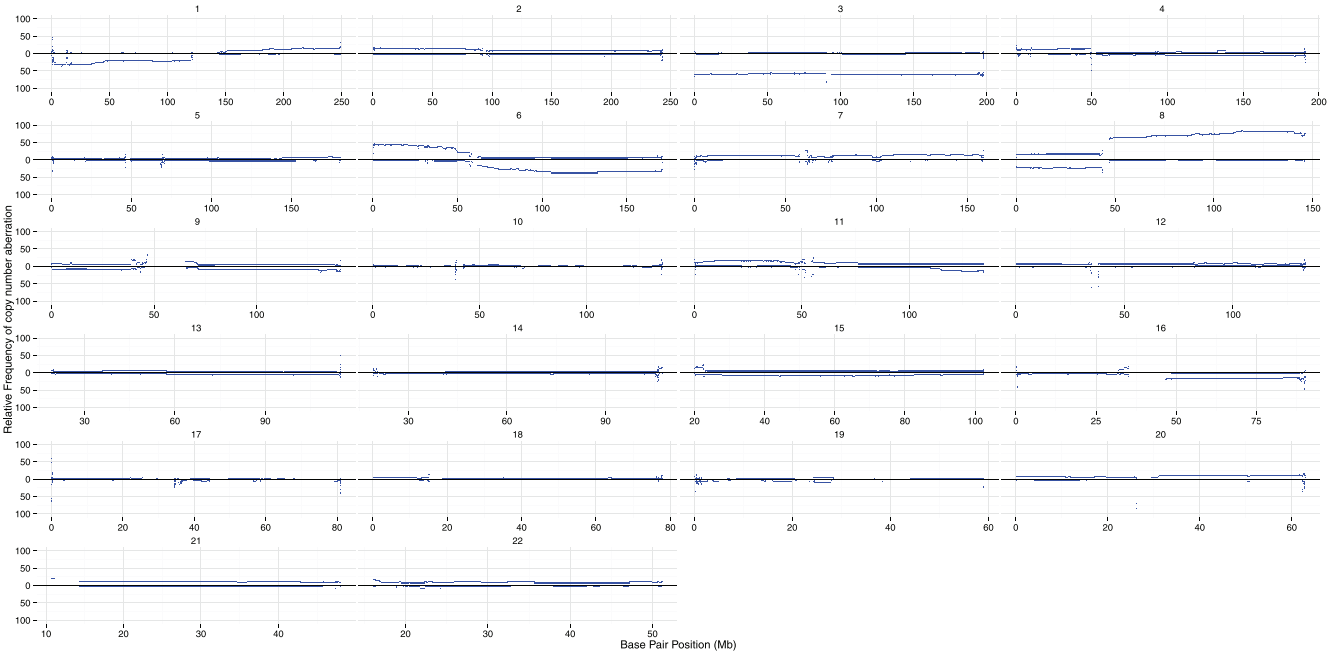

Figure 2. Whole genome copy number aberration frequencies. Each autosome is indicated by a separate graph (1–22). The *y*-axis indicates relative frequency of copy number aberration within a clade: 0 indicates absence of copy number aberration. Deletions are below 0 and amplifications above 0. The *x*-axis indicates genomic position.

Table 2. Genomic Regions of the Most Frequent Amplifications and Deletions in Tumors Studied

Region	Amplification Count
8: 113865970–114758168	42
8: 111051403–112290740	42
8: 112296230–113859094	42
8: 114758203–131842636	42
8: 131860807–137156450	42
8: 137166576–140645504	42
8: 109776218–111047461	39
8: 137158556–137163816	42
8: 140650804–140662811	39
8: 143784500–144056784	36
8: 108400823–108626828	36
Region	**Deletion Count**
20: 26295705–26300032	**41**
3: 90318628–90428286	**40**
3: 90194622–90313054	**39**
20: 26246086–26293985	**34**
3: 197947034–197947632	**33**
3: 196695508–196730413	**32**
17: 30571–31444	**31**
3: 221081–234309	**31**
3: 149268501–149270023	**31**
3: 162512683–162625366	**31**
3: 178550246–178568018	**31**

centromeres, which include long repeating elements, are likely to be artifacts and are indicated with a star.

Clade A was characterized by loss of the majority of chromosome 3 (monosomy 3) and the gain of 8q. There were no copy number aberrations on selected segments of chromosomes 1, 5, 7, 8, 9, 10, 11, 14, 15, 16, 17, 18, 19, and 22 (Table 4).

Clade B demonstrated gains on 6p, as well as specific gains on 8q. It was also the clade most likely to have amplifications on 11 and 22. There were no copy number aberrations on selected segments of chromosomes 3, 10, 13, 17, and 19 (Table 4).

Clade C was defined by deletions on 6q. Additionally, it was most likely to have deletions on 1 and did not have any large copy number aberrations on chromosome 8. Chromosome 21 was entirely copy neutral for all samples within the clade. All other chromosomes had some copy number aberration in at least one of the samples in the clade (Table 4).

The gross genomic profile of each clade with respect to copy number aberrations is shown in Figure 4. Regions highlighted in blue are statistically associated with tumor clade, as determined by the Fisher's exact test.

The genes *GNAQ* and *GNA11* were predominantly copy neutral in all clades, with no difference in copy number aberrations by clade ($P = 0.10$, Fisher's exact test; Table 5). Similarly, the *SF3B1* gene was mostly copy neutral in all clades ($P = 0.04$, Fisher's exact test). However, in segments containing the *BAP1* gene, copy number aberrations were aberrant in all cases of clade A and copy neutral in clades B and C ($P < 0.01$, Fisher's exact test).

Hypothetical Ancestral Reconstruction

The genomic events characterizing the evolutionary path of uveal melanoma are summarized in Figure 5. From a normal diploid melanocyte, there is a small group of tumors (clade C, 6.1%) that loses a large portion of chromosome 6q. A few tumors within this group subsequently lose almost all of chromosome arm 1p. Clade C tumors do not develop any copy number aberrations on 8q, either deletions or amplifications, and some tumors develop additional copy number aberrations on other chromosomes, but in no discernible pattern.

In an alternate path, the vast majority of tumors (clades A and B, 91.9%), gain a copy of the telomeric half of 8q. A majority of these tumors (clade A) then subsequently lose a copy of chromosome 3, as well as duplicate the centromeric half of 8q. The other tumors (clade B) gain copies of 6p, as well as regions on 11p and 22q.

Discussion

Given the clinical infeasibility of sampling tumors at various stages of development, statistical analysis of genomic data provides a practical means for inferring tumor evolution. Our study uses a novel modeling strategy, increasingly being used within the field of evolutionary biology, to interpret data generated by new high-resolution assays.[19–21]

The population included in this study was representative of populations included in prior uveal melanoma series. In other words, our series included older white patients with similar rates of metastasis.[22] Thirty-eight of the 57 samples were discarded due to inability to estimate copy number profiles. The discarded samples were not significantly different from those samples that were analyzed in terms of their clinical features or patient characteristic, and therefore, the findings of this study are not likely to be biased for that reason (Table 1).

Previous studies have demonstrated that 8q gains occur in approximately 60% of tumors, whereas our study identified these gains in 92%.[23,24] Several explanations exist for this observed difference. First, previously published data regarding 8q gains come from either FISH studies, which target a single region,[24] or karyotyping studies,[23] which rely on visual examination of bands. The resolution of such assays is at the level of the chromosome arm,[25] whereas the microarray techniques used in the present study provide significantly higher resolution. Second, our observation of 92% includes both partial and whole arm gains, as opposed to only whole arm gains reported in previous studies. Third, the small sample size of our series could contribute to the observed difference. Regardless of whether or not the present series is biased toward tumors with 8q gains, the resulting inferred evolutionary tree would not be altered, because it estimates relationships between tumors, independent of the number of samples in each clade.

This work identified three major clades: clade A, clade B, and clade C. The organization of tumors into clades by copy number profiles does not depend on the number of tumors within each group, only the copy number profile itself. Clade assignment, although associated with metastasis, was not a perfect predictor of this event. Clade A was composed of 29 tumors, 20 of which were metastatic (69.0%). Clade B had 16 tumors, two of which were metastatic (12.5%), and clade C had three tumors, one of which was metastatic (33.3%; Table 3). The designation of metastatic status represents what has been clinically observed to date, leaving open the possibility for "nonmetastatic" tumors to metastasize with extended follow-up. The median follow-up duration was similar between clades (38.0, 61.0, and 53.0 months for clades A, B, and C, respectively). Shorter follow-up duration in clade A was due to metastatic death in 69.0% of cases. As 80% of mortality in uveal melanoma occurs within the first 5 years,[22] median follow-up of 61.0 and 53.0 months in clades B and C, respectively, is adequate for metastasis to manifest in the vast majority of cases.

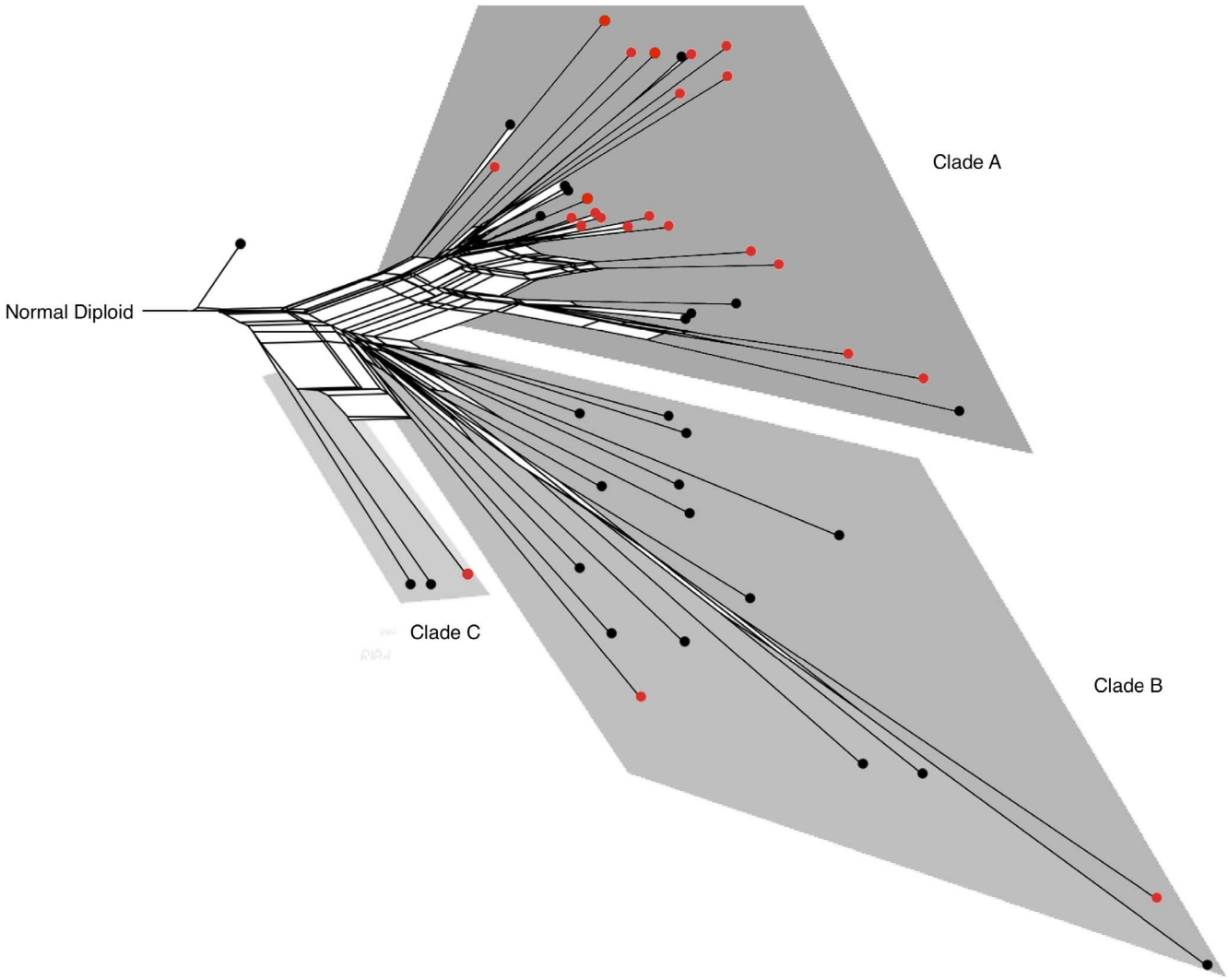

FIGURE 3. Estimated phylogenetic network (neighbor-net) of uveal melanoma by genomic copy number aberration. Each sample is represented as a node on the graph. Evolutionary relations are represented by an edge on the graph. Nodes are *red* if the sample was metastatic and *black* if they were not metastatic. Clades are identified by *gray shading*.

The SNP microarray can only reveal information about what is assayed, and the test sample may not be representative of the entire tumor, due to heterogeneous cell populations.[26,27] Sampling may therefore explain why some tumor samples were metastatic within an otherwise nonmetastatic clade.

Even though these tumors were located in different regions within the uveal tract (choroid only versus ciliary body ± iris or choroid), there was only a borderline association between location and clade ($P = 0.05$).

Clade A was characterized by monosomy 3 and amplification on 8q, clade B by duplication of 6p and 8q, and clade C by deletion of 6q, among other copy number aberrations. Because copy number aberrations common to clades A and B include duplications on 8q, it is inferred that these tumors followed a similar initial process of tumorigenesis. Distinct patterns of additional copy number aberrations indicate that these clades have divergent progression. The profiles of clades A and B largely agree with previous genomic studies of uveal melanoma in associating chromosomal copy number aberrations with metastatic status, further supporting the validity of our clade identification.[28,29]

Copy number aberrations on the *GNAQ*, *GNA11*, and *SF3B1* genes were mostly copy neutral within clades, with no difference in copy number aberration between clades (Table 5). These results can be explained by the fact that *GNAQ*, *GNA11*, *BAP1*, and *SF3B1* genes usually demonstrate point mutations in uveal melanoma.[4,5,7,30] These point mutations are not expected to be detected by our SNP microarray (Illumina Human660W-Quad v1.0 BeadChip) as the probes were not specifically designed to target these mutations. In contrast, segments containing the *BAP1* gene showed significant differences in copy number aberrations between clades, wherein all cases were aberrant in clade A and copy neutral in clades B and C, perhaps detecting loss of large segments of chromosome 3 rather than specific point mutations of the *BAP1* gene.

Previous studies have identified at least two subtypes of uveal melanoma (low and high metastatic risk). These can be differentiated by various techniques. For example, histopathology can separate low-grade spindle cell melanoma from more aggressive epithelioid tumors.[31] Risk stratification can also be accomplished through gene sequencing studies,[5] gene expression studies demonstrating correlation across histopathologic characteristics, and chromosomal aberrations identified by FISH and SNP.[32–34] A previous study that examined microsatellite array data suggested that monosomy 3 and loss of 6p defined two distinct pathways of uveal melanoma evolution,

Table 3. Demographic and Clinical Information About Clades

Parameter	Clade A ($n = 29$)	Clade B ($n = 16$)	Clade C ($n = 3$)	*P* Value
Age, mean (SD)	66.9 (13.7)	57.5 (15.3)	63.7 (11.2)	0.17
Sex				
Male	15	11	2	
Female	14	5	1	0.57
Location				
Choroidal only	10	11	2	
Ciliary body ± iris or choroid	19	5	1	0.05
AJCC classification				
1a	1	1	0	
2a	2	5	0	
2b	3	0	0	
3a	5	3	2	
3b	7	2	1	
4a	2	2	0	
4b	9	3	0	0.36
Metastasis				
Present	20	2	1	
Absent	9	14	2	<0.01
Median follow-up time, months	38.0	61.0	53.0	0.05

Table 4. Genomic Regions Amplified or Deleted in ≥80% of the Identified Clades

Clade	Amplifications	Deletions
Clade A, $n = 29$	8: 46840092–146203412	3: 63411–197780227 3: 197943361–197947632 20: 26295705–7059794763*
Clade B, $n = 16$	6: 213426–26765906 6: 26906789–32450089 6: 32536348–34204064 6: 34318837–34673149 6: 37836673–41290719 6: 43710756–46130385 8: 109776218–140662811	20: 26246086–0864066281
Clade C, $n = 3$		3: 90194622–224066281 6: 86234835–132797275 6: 167488211–167489090 10: 38792507–38871808* 20: 26246086–086 871808*

* Genomic events that occur within centromeric regions. These events are likely to be artifacts, arising from the repeated sequences.

with 8q gain involved in both pathways.[35] The study used whole chromosome arm level data and ad hoc methods to ascertain the specific ordering of mutations, whereas our study took advantage of higher resolution microarray data and well-established evolutionary biology methodology. Our analysis more specifically identified the time course of important genomic events in uveal melanoma tumorigenesis. Additionally, the present study provides evidence for a newly described (third) potential evolutionary pathway represented by the minor clade of tumors (clade C: 3/49; 6.1%; Fig. 3). The distinct patterns of copy number status, specifically deletions on chromosome 6q, and the different rate of metastasis, indicate that clade C may well represent a third subtype to add to the original two subtype model of uveal melanoma.[36] Minor subgroups of uveal melanoma are being identified in other series with extended follow-up. In many cases, these tumors manifest with late onset of metastasis.[37]

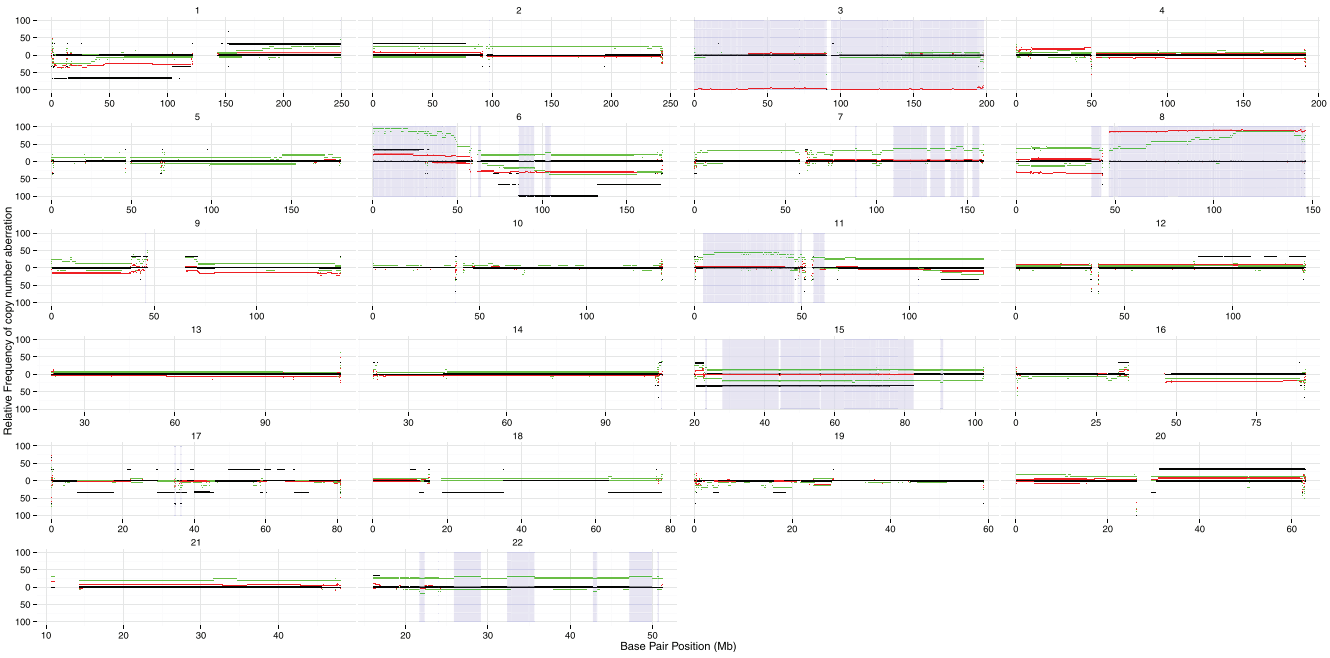

Figure 4. Whole genome copy number aberration frequencies by clade. Each autosome is indicated by a separate graph (1–22). Clade A is indicated by the *red line*, clade B by the *green line*, and clade C by the *black line* within each autosome. The *y*-axis indicates relative frequency of copy number aberration within a clade: 0 indicates absence of copy number aberration. Deletions are below 0 and amplifications above 0. The *x*-axis indicates genomic position. Regions shaded in *blue* are statistically associated ($P < 0.05$) with a clade by the Fisher's exact test, using a Benjamini-Hochberg correction for multiple testing.

Investigative Ophthalmology & Visual Science

Table 5. Copy Number Aberrations of Regions Containing Key Driver Genes of Uveal Melanoma

Gene	Clade A, $n = 29$	Clade B, $n = 16$	Clade C, $n = 3$	*P* Value
GNAQ				
Deletion	5	0	0	
Copy neutral	24	14	3	
Amplification	0	2	0	0.10
GNA11				
Deletion	0	1	0	
Copy neutral	29	15	3	
Amplification	0	0	0	0.40
BAP1				
Deletion	27	0	0	
Copy neutral	0	16	3	
Amplification	2	0	0	<0.01
SF3B1				
Deletion	1	0	0	
Copy neutral	28	12	3	
Amplification	0	4	0	0.04

The evolutionary framework used in this study can also be used to study copy number profiles of systemic metastases, which can then be traced back to the lineage of the primary tumor. Additionally, this framework allows for studying the evolutionary relationships of subpopulations of cells within the same tumor, which is widely recognized to be an important aspect of cancer evolution.[38] Finally, the relationship between the tumors and their cell lines can be clearly elucidated as there is general controversy about the validity of data derived from cell lines that are known to have highly aberrant gene expression and copy number profiles.

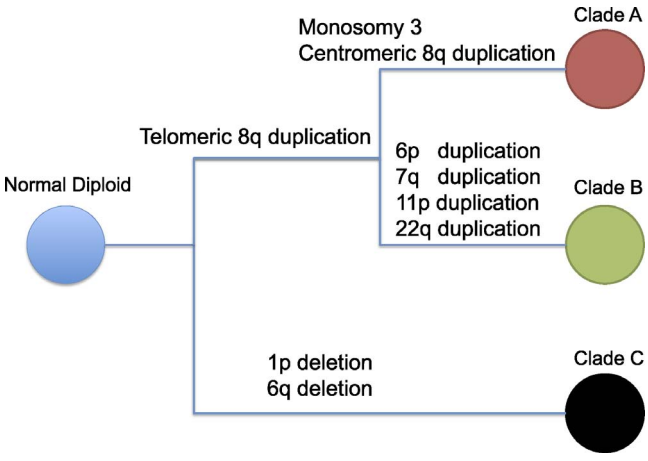

Figure 5. Stylized summary of evolutionary path of subtypes of uveal melanoma. Clade A was characterized by monosomy 3 and amplification of the whole arm of 8q, clade B by duplication of 6p and telomeric 8q, and clade C by deletion of 6q, among other copy number aberrations. Because copy number aberrations common to clades A and B include duplications on telomeric 8q, it is inferred that these tumors followed a similar initial process of tumorigenesis; however, distinct patterns of additional copy number aberrations indicate that these clades have divergent progression. The profiles of clades A and B largely agree with previous genomic studies of uveal melanoma in associating chromosome arm level copy number aberrations with metastatic status, supporting the validity of our clade identification.

From the copy number profiles, genetic copy number aberration distances were calculated between tumors, and these distances were used to infer an evolutionary tree. A distance-based method has two strengths. First, distance-based methods are less computationally demanding and are therefore flexible enough to use the entire tumor genome instead of a smaller subset of copy number events. In this way, there is maximal leverage of the genome-wide information. Second, these methods are rapid to implement and therefore provide a user-friendly approach to the problem. However, distance-based approaches are limited in their ability to construct ancestral states, as the methods do not calculate the likelihood of possible ancestral states.

There were a few limitations to the study, which were consequences of using SNP microarrays. First, SNP microarray analyzes the abundance of specific genomic regions, and it is therefore unable to capture other types of genomic mutations, such as copy neutral inversions or point mutations. There is evidence that such mutations are likely involved in tumorigenesis.[5] Second, our analysis cannot identify possible epigenetic events that may also play a role in the progression of uveal melanoma.[39]

The next step in our work will be to study additional samples using other platforms so that more robust copy number signatures for each major clade can be validated. This will also allow further characterization of potential minor clades. In the future, work focused on the identification of the genes residing within each clade needs to be performed.

Applying an evolutionary framework to the uveal melanoma genome reveals that there are distinct subtypes of uveal melanoma and that these subtypes resemble each other in their initial development, but that they diverge along their evolutionary course. Our data also suggest that there is little overlap in the subtypes of uveal melanoma after divergence (identified as clades A and B). These distinct subtypes are not likely to crossover or transform from one major clade to another major clade.

Acknowledgments

Marcus Riester and David Wypij provided helpful comments at early stages of the research.

Supported by FALK trust (Chicago, IL, USA), Ratner Foundation (New York, NY, USA), and in part by a Cole Eye Institute, Research to Prevent Blindness Unrestricted Grant.

Disclosure: **N. Singh**, None; **A.D. Singh**, None; **W. Hide**, None

References

1. Kujala E, Mäkitie T, Kivelä T. Very long-term prognosis of patients with malignant uveal melanoma. *Invest Ophthalmol Vis Sci*. 2003;44:4651–4659.
2. Harbour JW, Chao DL. A molecular revolution in uveal melanoma: implications for patient care and targeted therapy. *Ophthalmology*. 2014;121:1281–1288.
3. Onken MD, Worley LA, Long MD, et al. Oncogenic mutations in GNAQ occur early in uveal melanoma. *Invest Ophthalmol Vis Sci*. 2008;49:5230–5234.
4. Van Raamsdonk CD, Griewank KG, Crosby MB, et al. Mutations in GNA11 in uveal melanoma. *N Engl J Med*. 2010;363:2191–2199.
5. Harbour JW, Onken MD, Roberson ED, et al. Frequent mutation of BAP1 in metastasizing uveal melanomas. *Science*. 2010;330:1410–1413.
6. Martin M, Masshofer L, Temming P, et al. Exome sequencing identifies recurrent somatic mutations in EIF1AX and SF3B1 in uveal melanoma with disomy 3. *Nat Genet*. 2013;45:933–936.

7. Roberson EDO, Anbunathan H, Onken MD, Worley LA, Harbour JW, Bowcock AM. Recurrent mutations at codon 625 of the splicing factor SF3B1 in uveal melanoma. *Nat Genet*. 2013;45:133–135.
8. Matatall KA, Agapova OA, Onken MD, Worley LA, Bowcock AM, Harbour JW. BAP1 deficiency causes loss of melanocytic cell identity in uveal melanoma. *BMC Cancer*. 2013;13:371.
9. Aminov RI, Mackie RI. Evolution and ecology of antibiotic resistance genes. *FEMS Microbiol Lett*. 2007;271:147–161.
10. Singh AD, Aronow ME, Sun Y, et al. Chromosome 3 status in uveal melanoma: a comparison of fluorescence in situ hybridization and single-nucleotide polymorphism array. *Invest Ophthalmol Vis Sci*. 2012;53:3331–3339.
11. Owzar K, Barry WT, Jung SH, Sohn I, George SL. Statistical challenges in preprocessing in microarray experiments in cancer. *Clin Cancer Res*. 2008;14:5959–5966.
12. Staaf J, Vallon-Christersson J, Lindgren D, et al. Normalization of Illumina Infinium whole-genome SNP data improves copy number estimates and allelic intensity ratios. *BMC Bioinformatics*. 2008;9:409.
13. Popova T, Manié E, Stoppa-Lyonnet D, Rigaill G, Barillot E, Stern MH. Genome Alteration Print (GAP): a tool to visualize and mine complex cancer genomic profiles obtained by SNP arrays. *Genome Biol*. 2009;10:R128.
14. Hsiao LL, Jensen RV, Yoshida T, Clark KE, Blumenstock JE, Gullans SR. Correcting for signal saturation errors in the analysis of microarray data. *Biotechniques*. 2002;32:330–332.
15. van de Wiel MA, Wieringen WN. CGHregions: dimension reduction for array CGH data with minimal information loss. *Cancer Inform*. 2007;3:55–63.
16. Huson DH, Bryant D. Application of phylogenetic networks in evolutionary studies. *Mol Biol Evol*. 2006;23:254–267.
17. Benjamini Y, Hochberg Y. Controlling the false discovery rate: a practical and powerful approach to multiple testing. *J R Stat Soc Series B Stat Methodol*. 1995;57:289–300.
18. Goldman M, Craft B, Swatloski T, et al. The UCSC Cancer Genomics Browser: update 2015. *Nucleic Acids Res*. 2015;43:D812–817.
19. Riester M. Stephan-Otto Attolini C, Downey RJ, Singer S, Michor F. A differentiation-based phylogeny of cancer subtypes. *PLoS Comput Biol*. 2010;6:e1000777.
20. Cheng YK, Beroukhim R, Levine RL, Mellinghoff IK, Holland EC, Michor F. A mathematical methodology for determining the temporal order of pathway alterations arising during gliomagenesis. *PLoS Comput Biol*. 2012;8:e1002337.
21. Haeno H, Gonen M, Davis MB, Herman JM, Iacobuzio-Donahue CA, Michor F. Computational modeling of pancreatic cancer reveals kinetics of metastasis suggesting optimum treatment strategies. *Cell*. 2012;148:362–375.
22. Singh AD, Turell ME, Topham AK. Uveal melanoma: trends in incidence, treatment, and survival. *Ophthalmology*. 2011;118:1881–1885.
23. Kilic E, Naus NC, van Gils W, et al. Concurrent loss of chromosome arm 1p and chromosome 3 predicts a decreased disease-free survival in uveal melanoma patients. *Invest Ophthalmol Vis Sci*. 2005;46:2253–2257.
24. van den Bosch T, van Beek JG, Vaarwater J, et al. Higher percentage of FISH-determined monosomy 3 and 8q amplification in uveal melanoma cells relate to poor patient prognosis. *Invest Ophthalmol Vis Sci*. 2012;53:2668–2674.
25. Kilic E, van Gils W, Lodder E, et al. Clinical and cytogenetic analyses in uveal melanoma. *Invest Ophthalmol Vis Sci*. 2006;47:3703–3707.
26. Mensink HW, Vaarwater J, Kilic E, et al. Chromosome 3 intratumor heterogeneity in uveal melanoma. *Invest Ophthalmol Vis Sci*. 2009;50:500–504.
27. Dopierala J, Damato BE, Lake SL, Taktak AF, Coupland SE. Genetic heterogeneity in uveal melanoma assessed by multiplex ligation-dependent probe amplification. *Invest Ophthalmol Vis Sci*. 2010;51:4898–4905.
28. McCannel TA, Burgess BL, Nelson SF, Eskin A, Straatsma BR. Genomic identification of significant targets in ciliochoroidal melanoma. *Invest Ophthalmol Vis Sci*. 2011;52:3018–3022.
29. Lake SL, Coupland SE, Taktak AF, Damato BE. Whole-genome microarray detects deletions and loss of heterozygosity of chromosome 3 occurring exclusively in metastasizing uveal melanoma. *Invest Ophthalmol Vis Sci*. 2010;51:4884–4891.
30. Van Raamsdonk CD, Bezrookove V, Green G, et al. Frequent somatic mutations of GNAQ in uveal melanoma and blue naevi. *Nature*. 2009;457:599–602.
31. McLean IW, Foster WD, Zimmerman LE. Uveal melanoma: location, size, cell type, and enucleation as risk factors in metastasis. *Hum Pathol*. 1982;13:123–132.
32. Tschentscher F, Husing J, Holter T, et al. Tumor classification based on gene expression profiling shows that uveal melanomas with and without monosomy 3 represent two distinct entities. *Cancer Res*. 2003;63:2578–2584.
33. Onken MD, Worley LA, Ehlers JP, Harbour JW. Gene expression profiling in uveal melanoma reveals two molecular classes and predicts metastatic death. *Cancer Res*. 2004;64:7205–7209.
34. van Essen TH, van Pelt SI, Versluis M, et al. Prognostic parameters in uveal melanoma and their association with BAP1 expression. *Br J Ophthalmol*. 2014;98:1738–1743.
35. Parrella P, Sidransky D, Merbs SL. Allelotype of posterior uveal melanoma: implications for a bifurcated tumor progression pathway. *Cancer Res*. 1999;59:3032–3037.
36. van Gils W, Kilic E, Bruggenwirth HT, et al. Regional deletion and amplification on chromosome 6 in a uveal melanoma case without abnormalities on chromosomes 1p, 3 and 8. *Melanoma Res*. 2008;18:10–15.
37. Landreville S, Agapova OA, Harbour JW. Emerging insights into the molecular pathogenesis of uveal melanoma. *Future Oncol*. 2008;4:629–636.
38. Heppner GH, Miller BE. Tumor heterogeneity: biological implications and therapeutic consequences. *Cancer Metastasis Rev*. 1983;2:5–23.
39. Merhavi E, Cohen Y, Avraham BC, et al. Promoter methylation status of multiple genes in uveal melanoma. *Invest Ophthalmol Vis Sci*. 2007;48:4403–4406.

Investigative Ophthalmology & Visual Science